

Experimental Realization of the Peregrine Soliton in Repulsive Two-Component Bose-Einstein Condensates

A. Romero-Ros,¹ G. C. Katsimiga,² S. I. Mistakidis^{3,4}, S. Mossman,^{5,6} G. Biondini^{7,8}
P. Schmelcher,^{1,9} P. Engels⁶, and P. G. Kevrekidis²

¹*Center for Optical Quantum Technologies, Department of Physics, University of Hamburg, Luruper Chaussee 149, 22761 Hamburg, Germany*

²*Department of Mathematics and Statistics, University of Massachusetts Amherst, Amherst, Massachusetts 01003-4515, USA*

³*ITAMP, Center for Astrophysics | Harvard & Smithsonian, Cambridge, Massachusetts 02138, USA*

⁴*Department of Physics, Harvard University, Cambridge, Massachusetts 02138, USA*

⁵*Department of Physics and Biophysics, University of San Diego, San Diego, California 92110, USA*

⁶*Department of Physics and Astronomy, Washington State University, Pullman, Washington 99164-2814, USA*

⁷*Department of Mathematics, State University of New York, Buffalo, New York 14260, USA*

⁸*Department of Physics, State University of New York, Buffalo, New York 14260, USA*

⁹*The Hamburg Centre for Ultrafast Imaging, University of Hamburg, Luruper Chaussee 149, 22761 Hamburg, Germany*



(Received 27 April 2023; revised 20 November 2023; accepted 12 December 2023; published 19 January 2024)

We experimentally realize the Peregrine soliton in a highly particle-imbalanced two-component repulsive Bose-Einstein condensate in the immiscible regime. The effective focusing dynamics and resulting modulational instability of the minority component provide the opportunity to dynamically create a Peregrine soliton with the aid of an attractive potential well that seeds the initial dynamics. The Peregrine soliton formation is highly reproducible, and our experiments allow us to separately monitor the minority and majority components, and to compare with the single component dynamics in the absence or presence of the well with varying depths. We showcase the centrality of each of the ingredients leveraged herein. Numerical corroborations and a theoretical basis for our findings are provided through three-dimensional simulations emulating the experimental setting and via a one-dimensional analysis further exploring its evolution dynamics.

DOI: [10.1103/PhysRevLett.132.033402](https://doi.org/10.1103/PhysRevLett.132.033402)

Introduction.—The fascination with rogue or freak waves has a time-honored history that can be argued to artistically go all the way back to Hokusai’s famous drawing of “The Great Wave off Kanagawa.” In a more quantitative form, for over half a century and since the early observations [1], the term “rogue wave” has been used for waves of elevation several times bigger than the average sea state. Further, and more well-documented occurrences of rogue waves have arisen in recent years and, in particular, since the notable observation of the so-called Draupner wave [2].

Recent progress has been catalyzed by a sequence of remarkable experiments in nonlinear optics, enabling the observation of rogue waves via novel detection techniques [3] and their practical use, e.g., for supercontinuum generation [4], and continued through a sequence of detailed analyses of related waveforms [5–9]. One candidate solution for rogue waves appearing in nature is the Peregrine soliton (PS) [10]. Subsequently, both fundamental, but also more complex (higher-order) rogue-wave patterns were observed in highly controlled fluid experiments [11–13], including the very recreation of the Draupner wave [14]. In turn, this progress prompted related

investigations in other fields, including plasmas [15–17], and the associated activity has more recently been summarized in a number of related reviews [18–23].

Bose-Einstein condensates (BECs) [24,25] have constituted a fertile playground where various types of nonlinear waves, including bright and dark solitons, vortices, vortex lines, and rings, among others [26], have been realized experimentally at a mean-field level. Importantly, the above list also extends to numerous salient features of attractive condensates, including the formation of bright solitons [27], the modulational instability that may produce trains thereof [28–30], or the nature of their interactions and collisions [31]. Yet, to the best of our knowledge, the creation of one of the most quintessential nonlinear waveforms, i.e., the PS [10], a structure localized in time and space that emerges from a modulationally unstable background and decays back to it, has remained elusive. This situation may be attributed to numerous key factors associated with the fairly precise control needed to produce such an entity. Such factors include the structure’s modulationally unstable background, the temporally localized nature of its existence (together with the typically destructive imaging), and the “dimensionality reduction” from

three-dimensions (3D) to quasi-one-dimension (1D) and its impact on the resulting dynamics.

The aim of the present work is to overcome these major obstacles and report the first experimental observation of the PS in BECs. To do so, we leverage a number of crucial ingredients. Adapting the earlier idea of a two-component *self-defocusing* but immiscible setting consisting of a majority and a minority component creates an *effectively self-focusing medium* for the minority component [32,33]. This approach was utilized in two spatial dimensions to produce the well-known Townes soliton [34] that prompted the theoretical proposal of the PS realization [35].

We experimentally deploy a highly elongated trap geometry with an initial (weak) potential well at the condensate center. This well seeds the modulational instability of the minority component, providing a reproducible focal point for the spontaneous reshaping of the associated wave function into a PS, before eventually the modulationally unstable dynamics takes over and leads to the emergence of multiple peaks. Our numerical 3D and 1D analysis of the setting corroborates the nature of our experimental observations, while providing information about the phase structure. Moreover, we provide experimental evidence for the centrality of each of our above-mentioned experimental ingredients, since the absence of any one of them is detrimental to the PS formation.

Experimental results.—We experimentally demonstrate the formation of the PS in a ^{87}Rb BEC of $N \approx 9 \times 10^5$ atoms where all interatomic interactions are repulsive. Initially, the atoms occupy the single hyperfine state $|F, m_F\rangle = |1, -1\rangle$. The BEC is confined in a highly elongated harmonic trap with frequencies $(\omega_x, \omega_y, \omega_z) = 2\pi \times (2.5, 245, 258)$ Hz. The 100:1 aspect ratio of the optical trap ensures effectively 1D dynamics, leaving at most collective excitations (i.e., absence of any nonlinear

structure) along the transverse direction observed in experiment and confirmed numerically. An additional attractive optical potential is present in the central part of the BEC producing a small density hump in the center of the cloud; see Supplemental Material (SM) [36] for further details. This optical potential, characterized by waists $s_x \approx 13 \mu\text{m}$ and $s_y \approx 25 \mu\text{m}$ and approximate depth of 97 nK, is radially uniform but has a Gaussian shape along the long axis of the BEC. From this static initial condition with chemical potential $\mu \approx 97$ nK [36], the dynamics is initiated by rapidly transferring a small fraction ($\sim 15\%$) of the atoms to the $|2, 0\rangle$ state with a $55 \mu\text{s}$ microwave pulse, and transferring the remaining atoms to the $|1, 0\rangle$ state in a $102 \mu\text{s}$ rf pulse. Both pulses are applied uniformly across the whole BEC.

In the following, we focus on the dynamics of the $|2, 0\rangle$ hyperfine state (minority component) for which an effective self-focusing description applies. Snapshots of the corresponding density distributions are presented both in experiment and theory in Fig. 1. The experimental images [Figs. 1(a)–1(h)] include an additional 9 ms of time of flight to avoid image saturation of the high density peak. The initially prepared Gaussian hump in the center of the BEC is seen to evolve into a narrow, high peak flanked by two clear dips on either side, after approximately 65 ms [Figs. 1(c) and 1(g)]. These dips are a characteristic feature of a PS and are related to the formation of a π phase jump of the wave function in the peak region relative to the surrounding BEC, leading to destructive interference at the position of the dips (see also Fig. 3). Subsequently, the peak height decreases, leading to the emergence of side peaks and excitations on either side around 85 ms [Figs. 1(d) and 1(h)]. We note that the observed timescales are highly reproducible, indicating that the dynamics is a well-defined consequence of the initial conditions prepared

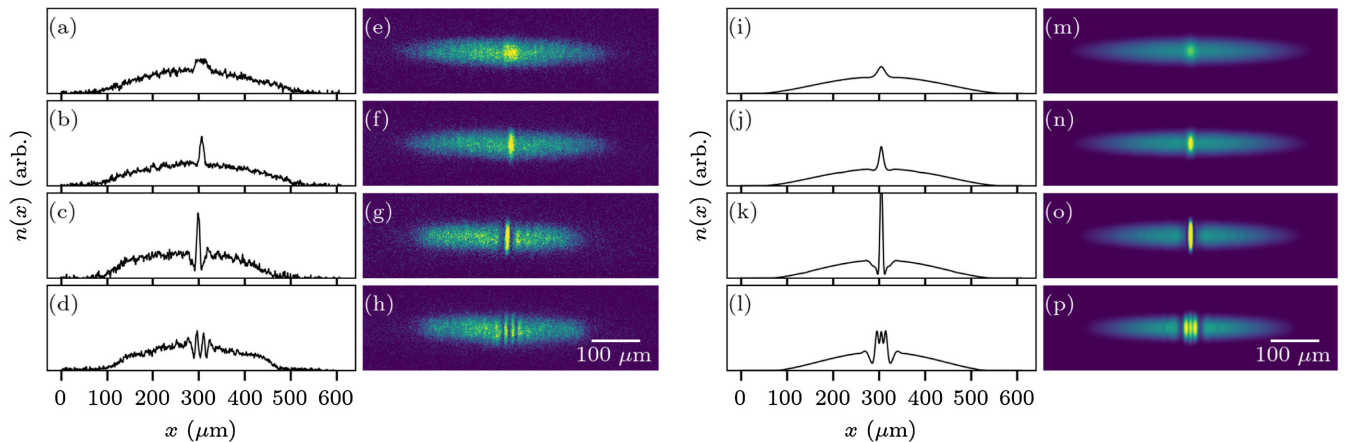


FIG. 1. Comparison between (a)–(h) experimental and (i)–(p) numerical observations for the emergence of the PS. (a)–(d) Cross sections of (e)–(h) showing single-shot absorption images after 10, 30, 65, and 85 ms of evolution, respectively, with an additional 9 ms of free expansion for imaging. (i)–(l) Cross sections of (m)–(p) represent the density profiles obtained from the 3D mean-field simulations under the experimental conditions. The vertical axis in the numerical images has been stretched for comparison with the experiment.

in the experiment. This is also confirmed by our 3D simulations [Figs. 1(i) to 1(p)], further discussed below.

Mean-field dynamics.—Following the experimental conditions, we consider a ^{87}Rb BEC in the aforementioned hyperfine states with a spin population imbalance of 85%–15%. To model the dynamical generation of the PS, we employ two coupled 3D Gross-Pitaevskii equations [24–26],

$$i\hbar\partial_t\Psi_F(\mathbf{r},t) = \left[-\frac{\hbar^2}{2m}\nabla_{\mathbf{r}}^2 + V(\mathbf{r}) + V_G(\mathbf{r}) + \sum_{F'=1}^2 g_{FF'}|\Psi_{F'}(\mathbf{r},t)|^2 \right] \Psi_F(\mathbf{r},t). \quad (1)$$

Here, $\Psi_F(\mathbf{r},t)$ is the 3D mean-field wave function with $F = 1, 2$ denoting each hyperfine state, $\mathbf{r} = (x, y, z)$, and m is the atomic mass. The external trap is given by $V(\mathbf{r}) = \sum_{\alpha=x,y,z} m\omega_{\alpha}^2\alpha^2/2$, and the coupling constants $g_{FF'} = 4\pi N_{F'}\hbar^2 a_{FF'}/m$ refer to the intra- ($F = F'$) and interspecies ($F \neq F'$) interaction strengths, with $a_{FF'}$ being the 3D s -wave scattering lengths, and N_F is the atom number in the F spin channel. Specifically, the scattering lengths corresponding to the experimental setup are $a_{11} = 100.86a_0$, $a_{22} = 94.57a_0$, and $a_{12} = a_{21} = 98.9a_0$, where a_0 designates the Bohr radius. These coefficients give rise to an *effective* attractive nonlinear coefficient $a_{\text{eff}} = a_{22} - a_{12}^2/a_{11} < 0$, allowing for a reduced single-component description of the minority component [32,33].

Consequently, our system now supports the emergence of focusing nonlinear phenomena such as the PS. Neglecting the transverse coordinate dependence, the form of the PS is given by [10]

$$\Psi_P(x,t) = \sqrt{P_0} \left[1 - \frac{4\left(1 + 2i\frac{t-t_0}{T_P}\right)}{1 + 4\left(\frac{x-x_0}{L_P}\right)^2 + 4\left(\frac{t-t_0}{T_P}\right)^2} \right] e^{i\frac{t-t_0}{T_P}}, \quad (2)$$

where $T_P/\hbar = L_P^2 m/\hbar^2 = 1/(|g_{\text{eff}}|P_0)$. Here, T_P and L_P are the characteristic scales of time and space of the PS solution, respectively. P_0 represents the background density of the minority component in a homogeneous system, and $g_{\text{eff}} = g_{22}^{(1D)} - (g_{12}^{(1D)})^2/g_{11}^{(1D)}$ denotes the effective 1D interaction in the single-component description; see also SM [36].

To dynamically seed the PS nucleation, we employ the optically induced Gaussian well $V_G(\mathbf{r}) = -V_0 \exp\{-2[(x/s_x)^2 + (y/s_y)^2]\}$. The widths and the potential depth V_0 are fixed in accordance with the experimental setup. Note that the transverse spatial profile of the Gaussian potential does not significantly affect the PS generation, in line with the experimental observations,

as long as its width is larger than the transverse spatial extent of the BEC.

We initially place all N atoms in the $|1, -1\rangle$ state and identify the ground state of this system in the presence of the optical well utilizing the time-independent version of Eq. (1). We then instantaneously transfer a fraction of typically 15% (85%) of the atoms to the $|2, 0\rangle$ ($|1, 0\rangle$) state, thus emulating the rf experimental process. Additionally, we approximately account for the experimental thermal fraction ($< 10\%$) and for the observed atom-loss rate in $|2, 0\rangle$ of around 0.23% per ms (see SM [36]). The two-component system is then allowed to evolve according to Eq. (1). Initially, the dynamical evolution of the stationary states described above entails the counterpropagating emission of sound waves with the subsequent PS generation reaching maximal amplitude around $t \approx 70$ ms [see the slightly earlier snapshots in Figs. 1(k) and 1(o)], before its structural deformation toward three equidistant peaks [Figs. 1(l) and 1(p)]. A clear agreement with the experimental PS realization and the overall dynamics [Figs. 1(a) to 1(h)] is observed. Any residual deviations in the intensity of the PS are principally traced back to the time of flight performed in the experiment but not taken into account in the simulations.

Controllability of Peregrine generation.—To unveil the necessary conditions for the formation of a PS, Fig. 2 presents a collection of various alterations of the experimental procedure discussed above. As a baseline for comparison, Figs. 2(a) and 2(g) show a PS beginning to form under the conditions described in Fig. 1 after 50 ms of evolution. If an identical experiment is performed but with a single-component cloud, no PS is observed [Figs. 2(b) and 2(h)], demonstrating the key role of interspecies interactions for the emergent dynamics. The deformation of the initially Gaussian bulge is due to expansion during time of flight. Specifically, the initial Gaussian shaped density hump spreads out, leading to sound wave pulses propagating away from each other. Also, when conducting experiments with the two-component mixture in the absence of the well, instability takes longer to set in and no PS forms within accessible timescales [Figs. 2(c) and 2(i)].

Having identified the presence of the optical well and the genuine two-component mixture as key ingredients, we can further elucidate their roles. Figures 2(d) and 2(j) show a mixture of 15% of atoms in the $|2, 0\rangle$ state embedded in a 85% background of atoms in the $|1, -1\rangle$ state [as opposed to $|2, 0\rangle$ and $|1, 0\rangle$ atoms used for Figs. 2(a) and 2(g)]. The dynamical generation of the PS is again clearly observed, although this mixture is characterized by a less attractive effective scattering length of $a_{\text{eff}} = -1.34a_0$ for the $|2, 0\rangle$ atoms, as compared to $-2.41a_0$ for the $|2, 0\rangle$ atoms embedded in a $|1, 0\rangle$ background. The formation of a PS, as discussed above, is not highly specific to some of the exact parameters of the Gaussian well, e.g., if the well

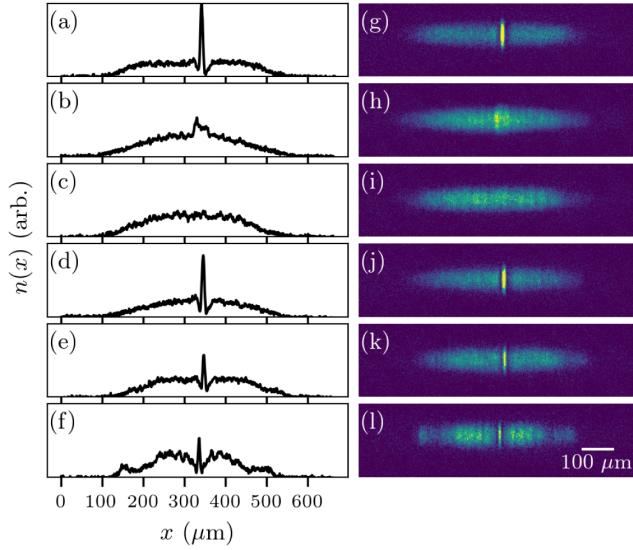


FIG. 2. Impact of the optical trap features on PS nucleation. (a), (g) Standard PS sequence after 50 ms of evolution. (b),(h) All atoms in a single component ($|1, 0\rangle$) showing no PS formation. (c),(i) Minority component prepared without the potential well leading to the absence of PS. (d),(j) A PS forming in the $|1, -1\rangle$ & $|2, 0\rangle$ mixture after 50 ms of evolution (instead of the $|1, 0\rangle$ & $|2, 0\rangle$ mixture). (e),(k) Well depth cut by half compared to panel (a), then 80 ms evolution. (f),(l) Well [with the same depth as in panel (a)] switched off at 20 ms, with the image taken after 110 ms (i.e., 90 ms after the well was switched off). For further details on the interplay of PS generation and the well characteristics see SM [36].

depth is reduced by a factor of two, the PS still emerges, but at later evolution times. In particular, in Figs. 2(e) and 2(k) the PS starts to manifest after 80 ms of evolution time, compared to the approximately 50 ms needed in the case depicted in Figs. 2(a) and 2(g).

Importantly, the PS can emerge even if the well is only present for a short time after the initial preparation of the mixture, and it is then switched off. Figures 2(f) and 2(l) showcase a pertinent example, where the well was switched off abruptly at 20 ms after the preparation of the atomic mixture, and the image was taken after an additional evolution time of 90 ms after the switch-off (see also the discussion in SM [36]). This comparison demonstrates that the continued presence of the potential well is not required: the well only serves to “seed” the relevant dynamics leading to the PS generation. The possibility to trigger the dynamics in a controlled way is a powerful feature of our experimental setting, which enables us to produce the PS in a highly repeatable way, making it possible to study its time evolution. The instrumental role played by the well is further elucidated through more elaborated numerical investigations of the impact of its characteristics provided in Fig. 3.

Further characterization of the Peregrine.—Leveraging the 1D nature of the PS, we additionally employ a 1D reduction of Eq. (1) to further numerically characterize the

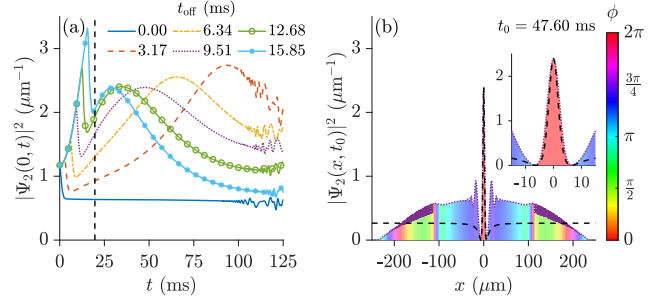


FIG. 3. 1D simulations of the minority component switching off the Gaussian well at indicated times before the expected nucleation of the PS (vertical black dashed line). (a) Time evolution of the central density, $|\Psi_2|^2$, of $|2, 0\rangle$. (b) Snapshot of $|\Psi_2|^2$ at the time instant of the PS formation after the well switch-off at $t = 9.51$ ms. The color gradient denotes the phase of Ψ_2 . A magnification of the central region in the inset showcases the good agreement between $|\Psi_2|^2$ and the analytical PS solution (2) (black dashed line) and the characteristic π phase jump between the core and the wings of the PS. The Gaussian well parameters used here are $V_0 = 60$ nK and $s_x = 4.8$ μm .

features of the PS in the context of these experiments. Here, we follow the experimental procedure described above while averaging over the transverse coordinates (see SM for details [36]).

Figure 3 demonstrates how the presence of the well assists in controllably seeding the emergence of the PS. In this particular case, we employ a well with $V_0 = 60$ nK and $s_x = 4.8$ μm . In Fig. 3(a) we present the time evolution of the central density of the minority component, $|\Psi_2(0, t)|^2$, when switching off the well at various time instants, t_{off} (see legend), before the PS nucleation would occur if the well was always present (vertical dashed line at $t = 19.68$ ms). In all cases, the PS emerges at some time, t_0 , after switching off the well. The exception is $t_{\text{off}} = 0$ ms (blue solid line), for which no PS forms. This supports the fact that, without the well, the above initial condition is not sufficient to form the PS. The earlier the switch-off, the later the PS emerges. Note that the process of switching off the well generates shock waves and their effect is visible after $t > 100$ ms.

To better understand the structure and properties of the PS, in Fig. 3(b), we provide an instantaneous density profile of $|2, 0\rangle$ and its corresponding phase (depicted by a color gradient) at t_0 when switching off the well at $t_{\text{off}} = 9.51$ ms. Additionally, we provide the profile of Eq. (2) with $P_0 = \max(|\Psi_2(x, t_0)|^2)/9$ (black dashed lines) to compare the emerging structure with the analytical PS solution. A close inspection of the central region of the condensate [inset of Fig. 3(b)] evinces the excellent agreement of the PS core among the two and the telltale π phase jump between the core and the wings of the waveform.

Conclusions.—We have experimentally demonstrated the dynamical formation of a PS in a two-component

BEC featuring a suitable mixture of repulsive interactions that emulate an effective attractive environment. This work shows how self-focusing interactions together with an attractive well as an effective catalyst cause a time-dependent localization to emerge from a modulationally unstable background resulting in the realization of a PS. Utilizing the attractive potential well it was possible to reproducibly and rapidly, i.e., comfortably within the condensate lifetimes, produce such wave structures in a highly controlled manner. A single repulsive component, not being modulationally unstable, is unable to produce such a phenomenon. Importantly, our experimental observations are in good quantitative agreement with 3D mean-field simulations. Simultaneously, a systematic 1D analysis revealed additional features of the phenomenology, such as the telltale phase gradient across the PS, and a detailed examination of the effect of switching off the well at different times.

Our platform paves the way for a closer inspection of rogue waves and higher-order rogue structures [12], or rogue waves in other ultracold atomic gas implementations such as intrinsically attractive BECs [27,29–31]. A natural question is the persistence of the PS generation in the dimensional crossover to 3D and how (parametrically) the 2D or 3D character comes into play. Another direction would be to extend these considerations to a larger number of components (e.g., spinor condensates [48,49]), to reveal the interplay of magnetic excitations and possibly emergent spin domains on the PS formation. Yet another possibility may be to study the formation of the mixed-bubble phase [50–52] that is inherently related to the presence of quantum fluctuations and occurs at the immiscibility threshold.

We acknowledge fruitful discussions lending context to this work at the Dispersive Hydrodynamics Program (2022) hosted by the Isaac Newton Institute for Mathematical Sciences. This material is based upon work supported by the U.S. National Science Foundation (NSF) under the Grants No. PHY-2110030 and No. DMS-2204702 (P. G. K.). S. I. M. acknowledges support from the NSF through a grant for ITAMP at Harvard University. P. E. acknowledges support from the NSF through Grant No. PHY-1912540 and from the Ralph G. Yount Distinguished Professorship at WSU. G. B. acknowledges support from the NSF through Grant No. DMS-2004987. The work of P. S. was funded by the Deutsche Forschungsgemeinschaft (German Research Foundation) under Grant No. SFB-925—Project No. 170620586.

[1] L. Draper, *Weather* **21**, 2 (1966).

[2] C. Kharif, E. Pelinovsky, and A. Slunyaev, *Rogue Waves in the Ocean*, Advances in Geophysical and Environmental Mechanics and Mathematics (Springer-Verlag, Berlin Heidelberg, 2009), 10.1007/978-3-540-88419-4.

- [3] D. R. Solli, C. Ropers, P. Koonath, and B. Jalali, *Nature (London)* **450**, 1054 (2007).
- [4] D. R. Solli, C. Ropers, and B. Jalali, *Phys. Rev. Lett.* **101**, 233902 (2008).
- [5] B. Kibler, J. Fatome, C. Finot, G. Millot, F. Dias, G. Genty, N. Akhmediev, and J. M. Dudley, *Nat. Phys.* **6**, 790 (2010).
- [6] B. Kibler, J. Fatome, C. Finot, G. Millot, G. Genty, B. Wetzel, N. Akhmediev, F. Dias, and J. M. Dudley, *Sci. Rep.* **2**, 463 (2012).
- [7] P. T. S. DeVore, D. R. Solli, D. Borlaug, C. Ropers, and B. Jalali, *J. Opt.* **15**, 064001 (2013).
- [8] B. Frisquet, B. Kibler, P. Morin, F. Baronio, M. Conforti, G. Millot, and S. Wabnitz, *Sci. Rep.* **6**, 20785 (2016).
- [9] A. Tikan, C. Billet, G. El, A. Tovbis, M. Bertola, T. Sylvestre, F. Gustave, S. Randoux, G. Genty, P. Suret, and J. M. Dudley, *Phys. Rev. Lett.* **119**, 033901 (2017).
- [10] D. H. Peregrine, *J. Aust. Math. Soc. Series B, Appl. Math.* **25**, 16 (1983).
- [11] A. Chabchoub, N. P. Hoffmann, and N. Akhmediev, *Phys. Rev. Lett.* **106**, 204502 (2011).
- [12] A. Chabchoub, N. Hoffmann, M. Onorato, and N. Akhmediev, *Phys. Rev. X* **2**, 011015 (2012).
- [13] A. Chabchoub and M. Fink, *Phys. Rev. Lett.* **112**, 124101 (2014).
- [14] M. L. McAllister, S. Draycott, T. A. A. Adcock, P. H. Taylor, and T. S. van den Bremer, *J. Fluid Mech.* **860**, 767 (2019).
- [15] H. Bailung, S. K. Sharma, and Y. Nakamura, *Phys. Rev. Lett.* **107**, 255005 (2011).
- [16] R. Sabry, W. M. Moslem, and P. K. Shukla, *Phys. Plasmas* **19**, 122903 (2012).
- [17] R. E. Tolba, W. M. Moslem, N. A. El-Bedwehy, and S. K. El-Labany, *Phys. Plasmas* **22**, 043707 (2015).
- [18] Z. Yan, *J. Phys. Conf. Ser.* **400**, 012084 (2012).
- [19] M. Onorato, S. Residori, U. Bortolozzo, A. Montina, and F. T. Arecchi, *Phys. Rep.* **528**, 47 (2013).
- [20] J. M. Dudley, F. Dias, M. Erkintalo, and G. Genty, *Nat. Photonics* **8**, 755 (2014).
- [21] D. Mihalache, *Rom. Rep. Phys.* **69**, 403 (2017), <https://rrp.nipne.ro/2017/AN403.pdf>.
- [22] J. M. Dudley, G. Genty, A. Mussot, A. Chabchoub, and F. Dias, *Nat. Rev. Phys.* **1**, 675 (2019).
- [23] A. Tikan, S. Randoux, G. El, A. Tovbis, F. Copie, and P. Suret, *Front. Phys.* **8** (2021).
- [24] C. J. Pethick and H. Smith, *Bose–Einstein Condensation in Dilute Gases*, 2nd ed. (Cambridge University Press, Cambridge, England, 2008), 10.1017/CBO9780511802850.
- [25] L. P. Pitaevskii and S. Stringari, *Bose-Einstein Condensation*, Oxford Science Publications No. 116 (Clarendon Press, Oxford; New York, 2003).
- [26] P. G. Kevrekidis, D. J. Frantzeskakis, and R. Carretero-González, *The Defocusing Nonlinear Schrödinger Equation: From Dark Soliton to Vortices and Vortex Rings*, Other Titles in Applied Mathematics (Society for Industrial and Applied Mathematics, Philadelphia, 2015), 10.1137/1.9781611973945.
- [27] L. Khaykovich, F. Schreck, G. Ferrari, T. Bourdel, J. Cubizolles, L. D. Carr, Y. Castin, and C. Salomon, *Science* **296**, 1290 (2002).

- [28] K. E. Strecker, G. B. Partridge, A. G. Truscott, and R. G. Hulet, *Nature (London)* **417**, 150 (2002).
- [29] K. E. Strecker, G. B. Partridge, A. G. Truscott, and R. G. Hulet, *New J. Phys.* **5**, 73 (2003).
- [30] P. J. Everitt, M. A. Sooriyabandara, M. Guasoni, P. B. Wigley, C. H. Wei, G. D. McDonald, K. S. Hardman, P. Manju, J. D. Close, C. C. N. Kuhn, S. S. Szigeti, Y. S. Kivshar, and N. P. Robins, *Phys. Rev. A* **96**, 041601(R) (2017).
- [31] J. H. V. Nguyen, P. Dyke, D. Luo, B. A. Malomed, and R. G. Hulet, *Nat. Phys.* **10**, 918 (2014).
- [32] Z. Dutton and C. W. Clark, *Phys. Rev. A* **71**, 063618 (2005).
- [33] B. Bakkali-Hassani, C. Maury, Y.-Q. Zou, É. Le Cerf, R. Saint-Jalm, P. C. M. Castilho, S. Nascimbene, J. Dalibard, and J. Beugnon, *Phys. Rev. Lett.* **127**, 023603 (2021).
- [34] R. Y. Chiao, E. Garmire, and C. H. Townes, *Phys. Rev. Lett.* **13**, 479 (1964).
- [35] A. Romero-Ros, G. C. Katsimiga, S. I. Mistakidis, B. Prinari, G. Biondini, P. Schmelcher, and P. G. Kevrekidis, *Phys. Rev. A* **105**, 053306 (2022).
- [36] See Supplemental Material at <http://link.aps.org/supplemental/10.1103/PhysRevLett.132.033402> for additional details on the experimental methods and complementary results, further comparisons between 3D mean-field simulations and experiment, and the parametric dependence of the PS generation, which includes Refs. [37–47].
- [37] M. Bertola and A. Tovbis, *Commun. Pure Appl. Math.* **66**, 678 (2013).
- [38] R. H. J. Grimshaw and A. Tovbis, *Proc. R. Soc. Math. Phys. Eng. Sci.* **469**, 20130094 (2013).
- [39] G. Biondini and D. Mantzavinos, *Phys. Rev. Lett.* **116**, 043902 (2016).
- [40] N. P. Proukakis and B. Jackson, *J. Phys. B* **41**, 203002 (2008).
- [41] P. Jain and M. Boninsegni, *Phys. Rev. A* **83**, 023602 (2011).
- [42] S. I. Mistakidis, G. C. Katsimiga, P. G. Kevrekidis, and P. Schmelcher, *New J. Phys.* **20**, 043052 (2018).
- [43] G. A. El', A. V. Gurevich, V. V. Khodorovskii, and A. L. Krylov, *Phys. Lett. A* **177**, 357 (1993).
- [44] L.-C. Zhao and L. Ling, *J. Opt. Soc. Am. B* **33**, 850 (2016).
- [45] V. E. Zakharov and A. A. Gelash, *Phys. Rev. Lett.* **111**, 054101 (2013).
- [46] G. Biondini, *Phys. Rev. E* **98**, 052220 (2018).
- [47] A. E. Kraych, P. Suret, G. El, and S. Randoux, *Phys. Rev. Lett.* **122**, 054101 (2019).
- [48] Y. Kawaguchi and M. Ueda, *Phys. Rep.* **520**, 253 (2012).
- [49] D. M. Stamper-Kurn and M. Ueda, *Rev. Mod. Phys.* **85**, 1191 (2013).
- [50] P. Naidon and D. S. Petrov, *Phys. Rev. Lett.* **126**, 115301 (2021).
- [51] S. I. Mistakidis, A. G. Volosniev, R. E. Barfknecht, T. Fogarty, T. Busch, A. Foerster, P. Schmelcher, and N. T. Zinner, *Phys. Rep.* **1042**, 1 (2023).
- [52] P. Stürmer, M. N. Tengstrand, and S. M. Reimann, *Phys. Rev. Res.* **4**, 043182 (2022).